Enhancing Accuracy and Efficiency: A Novel Implicit-Explicit Approach for Fluid Dynamics Simulation

Mahdi Moghadas Khorasani, Mohammad Hassan Djavareshkian[1]

Department of Mechanical Engineering, Faculty of Engineering, Ferdowsi University of Mashhad, P.O. Box 91775-1111, Iran

Abstract:

This study presents an innovative implicit-explicit time-stepping algorithm based on a first-order temporal accuracy method, addressing challenges in simulating all-regimes of fliud flows. The algorithm's primary focus is on mitigating stiffness inherent in the density-based "Roe" method, pivotal in finite volume approaches employing unstructured meshes. The objective is to comprehensively evaluate the method's efficiency and robustness, contrasting it with the explicit fourth-order Runge-Kutta method. This evaluation encompasses simulations across a broad spectrum of Mach numbers, including scenarios of incompressible and compressible flow. The scenarios investigated include the Sod Riemann problem to simulate compressible Euler equations, revealing the algorithm's versatility, and the low Mach number Riemann problem to analyze system stiffness in incompressible flow. Additionally, Navier-Stokes equations are employed to study viscous and unsteady flow patterns around stationary cylinders. The study scrutinizes two time-stepping algorithms, emphasizing accuracy, stability, and computational efficiency. Results demonstrate the implicit-explicit Runge-Kutta algorithm's superior accuracy in predicting flow discontinuities in compressible flow. This advantage arises from the semi-implicit nature of the equations, reducing numerical errors. The algorithm significantly enhances accuracy and stability for low Mach number Riemann problems, addressing increasing stiffness as Mach numbers decrease. Notably, the algorithm optimizes computational efficiency for both low Mach number Riemann problems and viscous flows around cylinders, reducing computational costs by 38% to 68%. The investigation extends to a two dimensional (2D) viscous flow over a circular cylinder, showcasing the method's proficiency in capturing complex flow behavior. Overall, this research advances the understanding of time discretization techniques in computational fluid dynamics, offering an effective approach for handling a wide range of Mach numbers while improving accuracy and efficiency.

[1] javareshkian@um.ac.ir

Keywords: Implicit-Explicit Runge-Kutta schemes, Incompressible flow, Stiffness, All-speed solver, Low Mach flows

1. Introduction

The unsteady compressible Navier-Stokes equations provide a fundamental mathematical framework for simulating a wide range of fluid mechanics applications in the fields of aerospace and mechanical engineering [1, 2]. The Navier-Stokes model provides a robust framework for describing the intricate dynamics of atmospheric and geophysical flows within the environment. Furthermore, this model holds substantial practical utility across diverse industrial sectors. It contributes to the optimization of wind and water turbines, the advancement of high-performance aircraft engines, and the design of cutting-edge automobiles. The governing equations, serving as the cornerstone for mathematical models across diverse scientific disciplines, are formulated based on the fundamental physical principle of conservation. These equations can be derived by applying the principles of mass conservation, which ensures the preservation of mass within a system; momentum conservation, accounting for the transfer and transformation of momentum in the presence of external forces; and total energy conservation, which encompasses the interplay between kinetic, potential, and internal energies within the system. The compressible Navier-Stokes equations can be decomposed into more elementary forms. For instance, the compressible Euler equations govern inviscid flows, while the incompressible Navier-Stokes equations emerge as the Mach number approaches zero under extreme conditions. The Mach number, signifying the connection between fluid velocity and the speed of sound, offers a comprehensive characterization of the fluid regime under consideration. The Mach number acts as a fundamental factor in discerning the properties of a fluid flow. In situations where the Mach number is less than 0.3 or the alterations in density are minimal, the flow is considered to be incompressible. Conversely, if

there are substantial variations in density and the Mach number exceeds 0.3, the flow is identified as compressible. Numerical techniques formulated for addressing problems associated with both high and low Mach numbers manifest distinct disparities due to the intrinsic characteristics of the governing equations. Put simply, when considering mathematical methods applied to resolving issues pertaining to high and low Mach numbers, noteworthy variations arise in the employed approaches. This is attributed to the governing equations, which delineate fluid flow behavior across different velocities, possessing distinct properties and necessitating specialized techniques for precise solutions. In high Mach number scenarios, the explicit upwind finite difference and Godunov-type finite volume methods are frequently employed. These techniques hold significant popularity in computational fluid dynamics (CFD) for scenarios involving high Mach numbers. Both the explicit upwind finite difference method and the Godunov-type finite volume method are specifically engineered to accurately simulate and resolve fluid flow issues under such conditions. [3, 4]. In the incompressible regime, the elliptic nature of the pressure field imposes a stringent limitation on the maximum allowable time step for low Mach number flows. The stability condition of explicit methods, represented by the CFL (Courant-Friedrichs-Lewy) criterion, intricately ties to the influence of sound speed. This influence assumes a prominent role as the Mach number approaches zero and governs the overall system behavior. Moreover, the study in [5] presents evidence of the detrimental impact of numerical viscosity on the accuracy of simulations involving slow waves generated by upwind-type schemes. It highlights the degradation in precision caused by such effects.The development of specialized methodologies aimed at addressing the challenges of the low Mach-number regime has yielded a rich and extensive body of research, exploring diverse paths of investigation. The primary strategy involves implementing preconditioning techniques. These approaches have been pioneered through

Chorin's utilization of the artificial compressibility technique [6]. The core concept involves multiplying time derivatives with an appropriate matrix. The primary objective is to manipulate the eigenvalues of the compressible system, mitigating the discrepancy between acoustic and fluid wave velocities, while also enhancing stability and the rate of convergence [7-11]. However, it is crucial to tackle issues stemming from computational instabilities caused by the eigenvector structure [12], along with occasional violations of the divergence-free velocity constraint. Addressing these concerns effectively is of paramount importance. In most cases, these techniques are confined to steady-state computations due to their involvement in modifying the time derivatives. When dealing with unsteady flows, the implementation of a dual time-stepping scheme [13, 14] can effectively restore temporal accuracy. As a result, an alternative pathway utilizing implicit methods for time discretization has been suggested to circumvent the acoustic CFL constraint and enhance the time step. Nevertheless, employing fully implicit methods requires solving large-scale nonlinear systems that impose a significant computational burden, and effectively managing numerical convergence becomes highly intricate. Furthermore, in numerous engineering applications, the coexistence of both high and low Mach regimes prevails, and their emergence during simulations cannot be predicted in advance. Thus, the development of numerical methodologies capable of effectively handling the entire spectrum of Mach numbers becomes imperative. Generally, fully implicit time-marching techniques entail higher computational costs compared to traditional explicit methods. However, fully implicit methods are preferred when the time-step restriction enforced by the CFL condition [15] is considerably smaller than the time-step required for achieving accurate simulations. Stiff systems exhibit significant discrepancies in time scales between their stiff and non-stiff components. Ensuring a stable and accurate solution demands meticulous handling and dedicated attention to the stiff part within the governing system.

Consequently, employing implicit discretization for the stiff component and explicit discretization for the non-stiff part effectively alleviates the time-step limitation imposed by the stiff element. Moreover, this approach offers the advantage of reduced computational expenses and implementation complexity when compared to fully implicit time-marching methods. Implicit-explicit (IMEX) methods have undergone extensive investigation in various research studies as promising substitutes for fully implicit techniques in simulating stiff problems. Ascher et al. [16] presented a comprehensive derivation of IMEX methods, grounded in linear multistep approaches, specifically designed to effectively simulate convection-diffusion equations. Furthermore, the authors developed third and fourth-order semi-implicit backward differentiation techniques that require only one computation of the non-stiff component for each time-step. Researchers in [17] proposed Implicit-Explicit (IMEX) techniques as a promising approach for modeling stiff equations, offering advantages over entirely implicit methods, as previously discussed in research. Additionally, these researchers developed third and fourth-order semi-implicit backward differentiation methods that require only one computation of the non-stiff component per time-step. These IMEX methods involve the combination of explicit Runge-Kutta (RK) and L-stable diagonally implicit RK methods for simulating convection-diffusion equations, necessitating the evaluation of four non-stiff terms at each time-step. Calvo et al. [18] formulated third and fourth-order IMEX methods by utilizing the Runge-Kutta (RK) technique, specifically tailored for convection-diffusion-reaction systems. Kupka et al. [19] extensively explored the mathematical properties and practical applicability of total-variation-diminishing IMEX Runge-Kutta methods for temporally integrating advection-diffusion equations commonly encountered in the simulation of double-diffusive convection. Boscarino et al. [20, 21] explored the practical application of IMEX methods for solving isentropic and full Euler equations using finite difference schemes.

Their discretization approach demonstrated excellent asymptotic preserving properties, making it suitable for a wide range of compressible and incompressible flow problems. They drew inspiration for the IMEX discretization concept from a previous work [22] and effectively derived an elliptic equation to handle pressure terms. The resulting system of nonlinear equations was efficiently solved using the Newton iteration method. Boscheri et al. conducted a research study in which they utilized a novel approach to partition segments with different stiffness properties of the Euler [23] and Navier-Stokes [24, 25] equations. They introduced an implicitly formulated elliptic equation to handle pressure computation. Moreover, to address time step constraints [26] arising from significant viscosity coefficients, they adeptly utilized implicit methods for solving the viscosity terms within the Navier-Stokes equations, ensuring simulation accuracy and efficiency. In an alternative study, the researchers examined the hydrodynamic [27-29] and stabili ty [30] characteristics of low Reynolds number flow over cylinders, specifically focusing on the i ncompressible formulation of the governing equations. The authors employed the Implicit-Explic it (Imex) scheme for time integration, wherein the pressure and diffusion terms were treated impl icitly. Through an exhaustive review of the existing literature on IMEX methods, we have revealed that despite their advantageous lower computational costs compared to fully implicit systems, at least one non-linear equation persists within the IMEX system. Yadav et al. [31] conducted a study in 2022 to simulate the compressible Navier-Stokes equations. In their study, a novel Implicit-Explicit (IMEX) Runge-Kutta method named 'Computationally Explicit Runge-Kutta (CERK)' was proposed to discretize the stiff terms. Remarkably, despite its implicit nature, this method effectively eliminates the need for computing coefficient matrix inversions. The efficacy of the proposed method was assessed across a spectrum of aeroacoustic viscous problems, in comparison with various Runge-Kutta methods. The findings demonstrated a significant reduction in the

stiffness of the system equations and a notable expansion of the stability domain. However, their study did not extend to consider inviscid flow and scenarios involving very low Mach numbers.

While the development of numerical methodologies for simulating unsteady flows in compressible fluid dynamics has witnessed significant progress, a critical gap remains in effectively addressing the entire spectrum of Mach numbers encountered in practical engineering scenarios. Current approaches often focus on either high Mach number regimes or low Mach number regimes, with limited attention given to seamlessly transitioning between these regimes within a single computational framework. This limitation stems from the inherent challenges posed by the varying stiffness properties and temporal characteristics of compressible flows under different Mach numbers. In response to this pressing research gap, our study proposes a novel advancement in Implicit-Explicit (IMEX) methods that transcend the confines of traditional approaches. Our innovation capitalizes on the intrinsic strengths of IMEX methods while circumventing their inherent limitation of retaining at least one non-linear equation within the system. Building upon the pioneering work by Yadav et al. [31], we introduce a computationally explicit Runge-Kutta (CERK) approach that not only reduces system stiffness but also eliminates the need for computationally intensive coefficient matrix inversions, thus enhancing efficiency without compromising accuracy. The distinguishing feature of our research lies in its multifaceted approach to seamlessly bridge the gap between high and low Mach number regimes. Firstly, while previous studies predominantly employed finite difference methods due to their simplicity, we expand the applicability of IMEX techniques by incorporating them within a finite volume framework. This enhancement enables us to tackle complex geometries and boundary conditions more effectively, leading to broader practical relevance. Furthermore, extending the CERK method to unstructured grids represents a pivotal departure from prior works primarily confined to

structured grids. By doing so, we unlock the potential for simulating real-world scenarios that demand refined spatial discretization strategies. A pivotal innovation lies in our endeavor to create an all-speed algorithm that excels across the entire spectrum of Mach numbers. By introducing a density-based upwind Roe scheme coupled with our new temporal discretization method, we enhance performance at low Mach numbers. Unlike traditional density-based algorithms that often require intricate preconditioning techniques, our implicit-explicit approach offers a straightforward yet effective alternative, potentially revolutionizing the treatment of low Mach number flows. By unifying the strengths of implicit and explicit methods through our IMEX formulation, our research positions itself as a significant departure from the conventional dichotomy between high and low Mach number simulations. Through an extensive numerical investigation encompassing both viscous and inviscid flows, we aim to substantiate the efficacy of our proposed method in terms of accuracy, stability, computational cost, and versatility across Mach number regimes. In doing so, our study strives to offer a holistic solution that not only addresses the current research gap but also propels the field of computational fluid dynamics toward a more unified and robust computational framework. In summary, our research stands out by presenting a comprehensive and innovative approach that transcends the limitations of existing methods. By harnessing the advantages of IMEX techniques, introducing novel adaptations for spatial discretization, and unifying all-speed capabilities, we contribute to a transformative shift in unsteady compressible flow simulations, promising increased accuracy and efficiency for a wide range of engineering applications.

In this research, we begin by presenting the governing equations for both viscous and inviscid flows in Section 2 and proceed to derive their non-dimensional forms. For spatial discretization, we employ the density-based "Roe" algorithm based on the finite volume method and introduce

higher-order spatial discretization schemes to address unstructured grids. Moving on to Section 3, we develop the comprehensive mathematical formulation of the computationally explicit Runge-Kutta algorithm, as utilized in the studies conducted by Yadav et al. [31]. Additionally, we extend this formulation to the fourth-order Runge-Kutta method for the Navier-Stokes and Euler equations. In Section 4, we thoroughly investigate the effectiveness of the newly developed computationally explicit Runge-Kutta method in comparison with the explicit fourth-order Runge-Kutta method. Numerical experiments are conducted for both viscous and inviscid flows, evaluating the performance of the implicit-explicit time discretization method in terms of robustness, stability, computational cost, and accuracy, compared to the explicit fourth-order Runge-Kutta method and findings from other references.

2. Governing equation

Hoffman and Chiang [32] presented the conservative form of the governing equations for two-dimensional Navier-Stokes flow as follows:

$$\frac{\partial Q_C}{\partial t}+\frac{\partial(F_c-F_v)}{\partial x}+\frac{\partial(F_c-F_v)}{\partial y}=0 \tag{1}$$

Within the given equation, Q_C is the conservative vector, F_c is inviscid flux vectors, and F_v is viscous flux vector. However, in the context of the Euler equation, the contribution of the viscous fluxes is disregarded and set to zero. To elaborate further, the definitions of both the viscous and inviscid fluxes in the Navier-Stokes equation are provided as follows:

$$\vec{Q}_c = \begin{bmatrix} \rho \\ \rho u \\ \rho v \\ \rho e_t \end{bmatrix}, \vec{F}_c = \begin{bmatrix} n_x(\rho u) + n_y(\rho v) \\ n_x(\rho u^2 + p) + n_y(\rho uv) \\ n_x(\rho uv) + n_y(\rho v^2 + p) \\ n_x(u(\rho e_t + p)) + n_y(v(\rho e_t + p)) \end{bmatrix},$$

$$\vec{F}_v = \begin{bmatrix} 0 \\ n_x \tau_{xx} + n_y \tau_{xy} \\ n_x \tau_{yx} + n_y \tau_{yy} \\ n_x \left(u\tau_{xx} + v\tau_{xy} + k\frac{\partial(T)}{\partial x} \right) + n_y \left(u\tau_{yx} + v\tau_{yy} + k\frac{\partial(T)}{\partial y} \right) \end{bmatrix} \tag{2}$$

$$p = \rho RT = (\gamma - 1)\left(\rho e_t - \frac{1}{2}\rho(u^2 + v^2) \right)$$

In Eq. (1), the variables are defined as follows: ρ represents the fluid density, u and v are the components of fluid velocity, p denotes the pressure, T is the absolute temperature, R represents the universal gas constant, μ is the dynamic viscosity of the fluid, e_t corresponds to the total energy of the fluid per unit mass, and K_t represents the thermal conductivity of the fluid. The expressions for the viscous stresses, τ_{xx}, τ_{xy} and τ_{yy}, are provided as follows:

$$\tau_{xx} = 2\mu\left[\frac{\partial u}{\partial x} - \frac{1}{3}\left(\frac{\partial u}{\partial x} + \frac{\partial u}{\partial y} \right) \right], \ \tau_{xy} = \tau_{yx} = \mu\left[\frac{\partial u}{\partial x} + \frac{\partial u}{\partial y} \right], \ \tau_{yy} = 2\mu\left[\frac{\partial v}{\partial x} - \frac{1}{3}\left(\frac{\partial u}{\partial x} + \frac{\partial v}{\partial y} \right) \right] \tag{3}$$

The system of Navier-Stokes equations is non-dimensionalized using reference values (ρ, L, C_∞, P_∞, μ_∞, T_∞), and the resulting non-dimensional quantities are obtained as follows:

$$x' = \frac{x}{L}, \ y' = \frac{y}{L}, \ u' = \frac{u}{C_\infty}, \ v' = \frac{v}{C_\infty}, \ \rho' = \frac{\rho}{\rho_\infty}, \ t' = \frac{t}{L/C_\infty}$$

$$, \ p' = \frac{p}{\gamma p_\infty}, \ \mu' = \frac{\mu}{\mu_\infty}, \ e_t' = \frac{e_t}{C_\infty^2}, \ T' = \frac{T}{T_\infty}, \ k' = -\frac{\mu'}{(\gamma - 1)Pr} \tag{4}$$

Upon substituting these values into the governing system of equations and omitting the superscripts, we obtain the following non-dimensional form:

$$\frac{\partial \rho}{\partial t}+\frac{\partial(\rho u)}{\partial x}+\frac{\partial(\rho v)}{\partial y}=0$$

$$\frac{\partial}{\partial t}(\rho u)+\frac{\partial}{\partial x}\left(\rho u^{2}+p\right)+\frac{\partial}{\partial y}(\rho u v)=\frac{M_{\infty}}{Re_{\infty}}\left[\frac{\partial}{\partial x}(\tau_{xx})+\frac{\partial}{\partial y}(\tau_{xy})\right]$$

$$\frac{\partial}{\partial t}(\rho v)+\frac{\partial}{\partial x}(\rho u v)+\frac{\partial}{\partial y}\left(\rho v^{2}+p\right)=\frac{M_{\infty}}{Re_{\infty}}\left[\frac{\partial}{\partial x}(\tau_{xy})+\frac{\partial}{\partial y}(\tau_{yy})\right] \quad (5)$$

$$\frac{\partial}{\partial t}(\rho e_{t})+\frac{\partial}{\partial x}(\rho u e_{t}+p u)+\frac{\partial}{\partial y}(\rho v e_{t}+p v)$$

$$=\frac{M_{\infty}}{Re_{\infty}}\left[\frac{\partial}{\partial x}(u\tau_{xx}+v\tau_{yy})+\frac{\partial}{\partial y}(u\tau_{yx}+v\tau_{yy})+k\frac{\partial T}{\partial x}+k\frac{\partial T}{\partial y}\right]$$

2.1. Spatial discretization of governing equation

In the spatial discretization of the system of equations, the Upwind "Roe" algorithm is employed specifically for unstructured mesh configurations [7]. The integral form of the Eq. (1) can be rewritten as follows:

$$\frac{d}{dt}(Q_{C})+\sum_{k=1}^{3}\vec{F}_{C_{K}}d\ell_{k}+\sum_{k=1}^{3}\vec{F}_{V_{K}}d\ell_{k}=0 \quad (6)$$

In the above equation, F_{C_k} is computed based on the "Roe" method using the following approach:

$$\vec{F}_{C_{K}}=\frac{1}{2}\left[\vec{F}_{C}\left(Q_{L}^{C}\right)+\vec{F}_{C}\left(Q_{R}^{C}\right)-\left|\tilde{A}_{i}\right|\Delta Q_{C}\right],\ \ \Delta Q_{C}=Q_{R}^{C}-Q_{L}^{C} \quad (7)$$

In Eq. (7), the matrix "$|A_i|$" represents the Jacobian matrix, and the values of the conservative variables Q_L and Q_R for the left and right states are determined using upwind interpolation. Subsequently, these values are employed to calculate the convective flux. The application of the limiter introduced in reference [33] enables the achievement of higher-order accuracy on unstructured grids through the careful reconstruction of flow variables. This advanced technique holds great significance in numerical simulations, as it allows for more precise representations of complex flow phenomena, leading to improved overall accuracy and reliability in computational fluid dynamics studies.

3. Temporal discretization schemes

3.1. Implicit-explicit Numerical scheme

The formulation of the implicit-explicit numerical scheme is based on the consideration of a stiff system of equations [34, 35], presented as follows:

$$\frac{\partial u}{\partial t} = F_1(u) + \zeta F_2(u) \tag{8}$$

where, $u \in R^m$, $F_i: R^m \to R^m$, i = 1 , 2 and $\zeta > 0$ represents the stiffness parameter and it may vary with time or space. In the current study, we have considered ζ as a constant stiffness parameter. The subsequent section focuses on the derivation and discussion of the implicit-explicit (CERK) methods specifically designed to address stiff systems. at first step, the value u^* is determined implicitly:

$$u^* = \Delta t \sum_{j=1}^{i-1} a_{ij} F_1(u^{(j)}) + \Delta t \sum_{j=1}^{i-1} \tilde{a}_{ij} \zeta F_1(u^{(j)}) - \Delta t \tilde{b}_{ij} \zeta u^*, \; i = 2,3,\ldots \tag{9}$$

In Eq. (9), the stiffness term is handled implicitly, effectively mitigating the stiffness exhibited by the system described in Eq. (8). Furthermore, in contrast to conventional IMEX methods, the variable u^* as defined in Eq. (9), obviates the need for coefficient matrix inversion, resulting in improved computational efficiency and reduced computational overhead. Eq. (9) can be restated in the following form:

$$u^* = \frac{\Delta t}{1 + \Delta t \tilde{b}_{ii} \zeta} \left[\sum_{j=1}^{i-1} a_{ij} F_1(u^{(j)}) + \Delta t \sum_{j=1}^{i-1} \tilde{a}_{ij} \zeta F_1(u^{(j)}) \right] \tag{10}$$

where, Δt is the time-step and $(\Delta t)_{eq} = \frac{\Delta t}{1+\zeta b_{ij}}$ represents the equivalent time-step utilized in Eq. (10). Due to $(\Delta t)_{eq}$ being smaller than the actual time-step Δt employed in the computations, it aids in mitigating the stiffness observed in Eq. (8). Other stages of the semi-implicit method are assessed as follows:

$$
\begin{aligned}
&u^{(1)} = u^{(n)} \\
&u^{(i)} = u^{(n)} + \frac{\Delta t}{1+\Delta t \tilde{b}_{ii}\zeta}\left[\begin{array}{l}\sum_{j=1}^{i-1} a_{ij} F_1\left(u^{(j)}\right) \\ +\sum_{j=1}^{i-1} \tilde{a}_{ij}\zeta F_2\left(u^{(j)}\right)\end{array}\right], \qquad \mathrm{i} = 2,\ldots,p+1 \\
&u^{(n+1)} = u^{(p+1)}
\end{aligned}
\tag{11}
$$

In this case, unlike conventional IMEX Runge-Kutta (RK) methods [17], the absence of a final explicit stage is evident, and the last equation in Eq. (11) solely denotes the updated values of unknowns at the $(n\ +\ 1)$ time step. In addition, the coefficients a_{ij} and b_{ij} are derived from the Butcher tableau [36] corresponding to the p-stage pth-order explicit RK method. The first-order IMEX Runge-Kutta type (Computationally explicit Runge-Kutta) method specifically tailored for stiff systems in Eq. (8) is derived as follows:

$$
\begin{aligned}
&u^{(1)} = u^{(n)} \\
&u^{(i)} = u^{(n)} + \frac{\Delta t}{1+\Delta t\zeta}\left[F_1\left(u^{(1)}\right) + F_2\left(u^{(1)}\right)\right] \\
&u^{(n+1)} = u^{(p+1)}
\end{aligned}
\tag{12}
$$

3.2. Fourth-order Explicit Runge-Kutta Method

The explicit fourth-order Runge-Kutta method is defined as follows [37]:

$$
\begin{aligned}
&u^{(1)} = u^{(n)} \\
&u^{(i)} = u^{(n)} + \tau_\ell\left[F_1\left(u^{(1)}\right) + F_2\left(u^{(1)}\right)\right] \\
&u^{(n+1)} = u^{(p+1)} \\
&\tau_\ell = \frac{1}{5-\ell} \qquad \ell = 1,\ldots,4
\end{aligned}
\tag{13}
$$

3.3. The implicit-explicit algorithm for the governing system of equations

The formulation of the first-order implicit-explicit (CERK) temporal discretization method for

the system of equations provided in Eq. (5) is outlined below:

$$
\begin{aligned}
(\rho u)^{(n+1)} &= (\rho u)^{(n)} - \frac{\Delta t}{\left(1+\Delta t\,\alpha_1 M^2\right)}\left[\left(\rho u^2 + p\right)_x^n + \left(\rho uv\right)_y^n - \frac{M_\infty}{Re_\infty}\left(\left(\tau_{xx}\right)_x^n + \left(\tau_{xy}\right)_y^n\right)\right] \\
(\rho v)^{(n+1)} &= (\rho v)^{(n)} - \frac{\Delta t}{\left(1+\Delta t\,\alpha_1 M^2\right)}\left[\left(\rho v^2 + p\right)_y^n + \left(\rho uv\right)_x^n - \frac{M_\infty}{Re_\infty}\left(\left(\tau_{xy}\right)_x^n + \left(\tau_{yy}\right)_y^n\right)\right] \\
(\rho)^{(n+1)} &= (\rho)^{(n)} - \Delta t\left[\left(\rho u\right)_x^{(n+1)} + \left(\rho v\right)_y^{(n+1)}\right] \\
(\rho e_t)^{(n+1)} &= (\rho e_t)^{(n)} - \frac{\Delta t}{\left(1+\Delta t\,\alpha_1 M^2\right)}\left[\begin{array}{l}\left(\rho e_t u + pu\right)_x^n + \left(\rho e_t v + pv\right)_y^n \\ -\frac{M_\infty}{Re_\infty}\left(\begin{array}{l}\left(u\tau_{xx} + v\tau_{xy}\right)_x^n + \left(u\tau_{yx} + v\tau_{yy}\right)_y^n \\ +\left(k\,\frac{\partial T}{\partial x}\right)^n + \left(k\,\frac{\partial T}{\partial y}\right)^n\end{array}\right)\end{array}\right]
\end{aligned}
\tag{14}
$$

In Eq. (14), the free parameter "$\alpha = 1$" is chosen. the superscript (n) designates the time-level, while the subscripts ($x\ and\ y$) are used to represent spatial derivatives with respect to the x and y directions, respectively. in this context, Yadav et al [31] established a sequential arrangement of the governing equations, optimizing the numerical solution process for the stiff problem. The momentum equations are prioritized and solved as the initial step, and the resulting updated flux values are utilized in the computation of the continuity equation. Subsequently, the energy equation is solved as the next step in the numerical solution process. After non-dimensionalizing the governing equation parameters with the reference speed of sound, it is observed that the convective terms in the momentum equation are of order $O(M^2)$, while the convective terms in the energy equation are of order $O(M)$. As a result, we select stiffness parameters for each equation that match the respective order of the convective terms. This research employs two numerical methods, namely the fourth-order Runge-Kutta method and the first-order implicit-explicit (CERK) scheme, to address a variety of benchmark numerical problems. The validity of the results is established by comparing them with either numerical simulations or experimental data. Additionally, we conduct

a comprehensive evaluation of the accuracy and computational efficiency of these two-time discretization approaches to gain valuable insights into their performance.

4. results

The primary objective of this section is a thorough and comprehensive analysis and evaluation of the performance of two distinct time discretization techniques: the fourth-order explicit Runge-Kutta method and the implicit-explicit algorithm. The specific aims encompass an investigation into their capabilities concerning stability domain considerations and computational efficiency. Through this rigorous examination, valuable insights into the advantages and limitations of each method are sought. To achieve these goals, a wide range of numerical simulations tailored for investigating incompressible flows in both one dimensional (1D) and two dimensional (2D) domains has been developed. Encompassing both viscous and inviscid flow regimes, these simulations include an examination of two Riemann problems aimed at simulating the Euler equations governing inviscid flow. The first Riemann problem scrutinizes a Mach number range from zero to one, involving compressible flow with multiple flow discontinuities. This scenario presents considerable challenges in terms of precision and robustness when implementing temporal discretization schemes. The focus of the second Riemann problem shifts to the formation of acoustic waves at extremely low Mach numbers. Here, the equation system's stiffness becomes critical, with particular attention directed towards the performance of implicit-explicit methods in such conditions. Additionally, the third scenario accounts for the impact of viscosity by solving the Navier-Stokes equations. The objective is to examine the steady and incompressible flow around a two-dimensional cylinder. This analysis is conducted by applying the mentioned time discretization schemes. Furthermore, an in-depth evaluation of essential factors significantly contributes to the comprehensive understanding of the system's behavior. By meticulously

scrutinizing these scenarios and their respective results, this research aims to advance the field's knowledge regarding the strengths and limitations of the studied time discretization techniques. This knowledge is essential for achieving accurate and efficient simulations in computational fluid dynamics applications.

4.1. Riemann 1D problems

This section employs the time integration methods introduced in the governing equations section to solve a sequence of classical Riemann problems. The initial conditions for these problems are graphically depicted in Fig. 1. Notably, the Sod Riemann problem is investigated using two distinct spatial discretization strategies. In the first scenario, a first-order spatial discretization approach is implemented, involving 499 elements along the horizontal direction. Conversely, the second case adopts a second-order spatial discretization scheme, utilizing 200 elements horizontally within the computational domain. Initiating with Dirichlet boundary conditions at both the initial and final points of the computational domain, reliant on provided initial values. The Sod Riemann problem emerges as a pivotal benchmark in gas dynamics [38], extensively employed to assess numerical methods' precision and efficiency in simulating shock waves and discontinuities. In this one-dimensional scenario, the issue encompasses a Mach number spectrum spanning from 0 to 1, involving the propagation of a shock wave, expansion fan, and contact discontinuity under the ideal gas assumption. The obtained numerical results for both the explicit Runge-Kutta method and the implicit-explicit numerical scheme, employing first-order and second-order spatial discretization, have undergone validation and comparison against reference data and the findings of other researchers. The numerical results of density, pressure, and velocity for both methods are showcased in Fig. 2 up to Fig. 7. Thorough validation and comparison have been conducted against reference data [24] as well as findings from other researchers to ensure the accuracy and reliability

of the presented results. The regions of expansion waves, contact discontinuity, and shock waves are distinctly delineated and visually emphasized using orange, blue, and red frames, respectively. This graphical representation enhances the clarity and prominence of each region for comprehensive analysis and interpretation. The primary errors identified in this study can be categorized into spatial and temporal domains. Regarding numerical dissipation in temporal discretization, the main focus of this study, the implicit-explicit Runge-Kutta method (CERK) demonstrates reduced numerical dissipation compared to the fully explicit Runge-Kutta method. This advantage arises from CERK's implicit treatment of the continuity equation during the solution process. Conversely, due to the use of first-order spatial discretization, the density-based Roe algorithm introduces significant numerical dissipation into the solution, resulting in smearing effects at numerical discontinuities. However, through the application of the semi-implicit approach, numerical dissipation is notably diminished, particularly in regions marked by expansion and compression waves (indicated by the red-framed region). This reduction leads to enhanced accuracy in computational results and alignment with reference solutions. Nonetheless, within the contact discontinuity region, outlined by the blue-framed area, the fourth-order Runge-Kutta method exhibits slightly superior accuracy to CERK. This discrepancy can be attributed to the temporal discretization order of the continuity equation. In the fourth-order Runge-Kutta method, the continuity equation is discretized using a fourth-order scheme, whereas the implicit-explicit Runge-Kutta method employs a first-order scheme for the same equation. In the subsequent phase of the investigation, the objective is to conduct a comprehensive examination and introduce more rigorous challenges for the temporal discretization algorithms. To achieve this, the computational grid resolution is deliberately reduced, and the spatial discretization order is simultaneously elevated to the second order. This enhancement contributes to a clearer and more

accurate research environment for a more effective comparison. As evident from Fig. 5 to Fig. 7, the increased spatial discretization order has notably improved computational accuracy for both examined temporal discretization algorithms. Consequently, the results from the temporal algorithms converge closely to each other, a direct outcome of the reduced numerical dissipation error. In the context of second-order spatial discretization, the most prominent numerical error is the dispersion error, leading to spurious oscillations in regions of shock and expansion discontinuities (highlighted by the orange and red-framed areas). The semi-implicit nature of the implicit-explicit method results in reduced numerical dissipation compared to the fourth-order Runge-Kutta method. Consequently, the oscillations arising from dispersion in the discontinuity regions are slightly amplified. Aligning with the first-order spatial discretization, the fourth-order Runge-Kutta method demonstrates superior accuracy in capturing the contact discontinuity region (highlighted by the blue-framed area), even with an increase in spatial accuracy compared to the implicit-explicit method. The numerical results from the simulation conducted by Boscheri et al. [23] are also depicted in Fig. 2 and Fig. 5. In their study, they utilized a computational grid consisting of 200 cells and employed a pressure-based implicit-explicit algorithm along with first and second-order temporal and spatial discretization. The outcomes demonstrate that the CERK method outperforms Boscheri's implicit-explicit algorithm in effectively capturing discontinuities and achieving higher computational accuracy. Table 2, presents a comprehensive comparison of the mentioned temporal discretization methods, with a particular focus on their stability and CPU time performance. This thorough analysis was conducted using a system equipped with the specified characteristics as outlined in Table 2. Notably, the Sod Riemann problem falls into the category of high Mach number problems and does not exhibit stiffness in its system of equations. Consequently, the stability domain of the fourth-order Runge-Kutta method surpasses that of the

first-order implicit-explicit method for this specific problem. Furthermore, the fourth-order Runge-Kutta method attains the final solution significantly faster, approximately 2 to 2.5 times quicker in terms of CPU time. The results presented effectively showcase substantial enhancements in both accuracy and performance when computing flow field properties such as density, velocity, and pressure. A logical correlation is evident between the extent of computational cost escalation and the corresponding enhancements in accuracy compared to the previous methods (Runge-Kutta). Notably, the incremental increase in computational cost proves to be relatively minor in comparison to the significant gains achieved in accuracy.

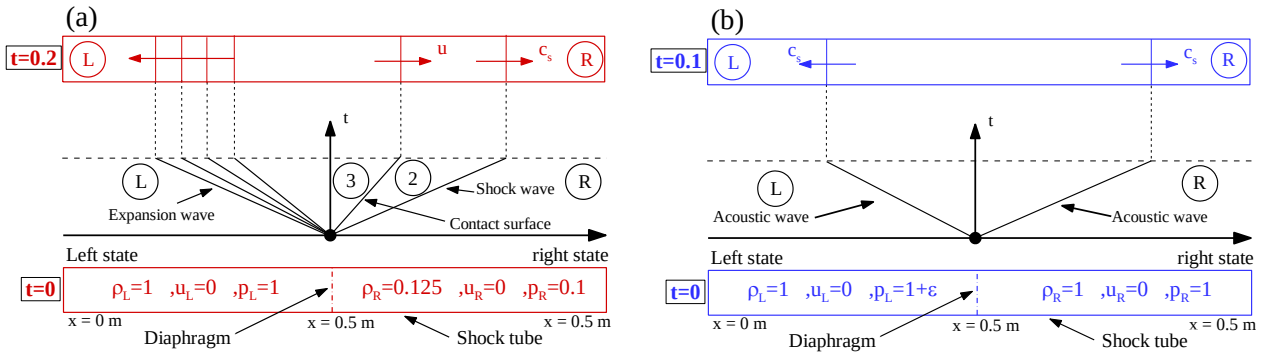

Fig. 1. Schematic of Riemann problems and the initial conditions for (a) Sod shock tube. (b) low Mach shock tube.

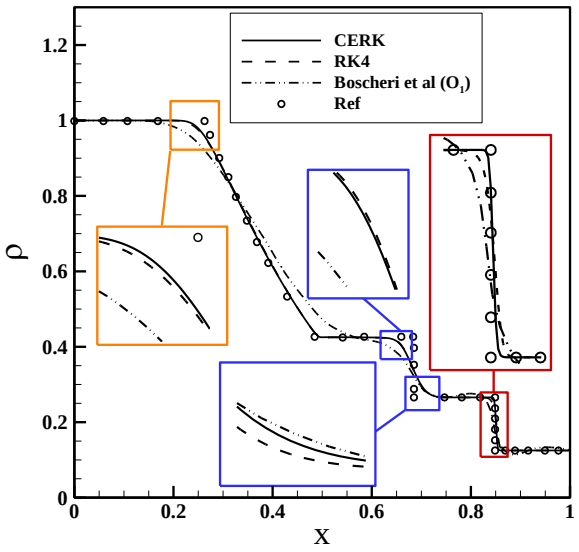

Fig. 2. Density variations in the Sod Riemann problem for first-order spatial discretization.

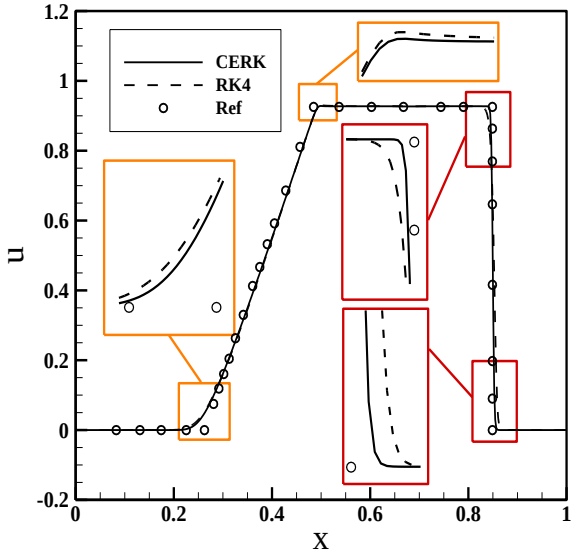

Fig. 3. Velocity variations in the Sod Riemann problem for first-order spatial discretization.

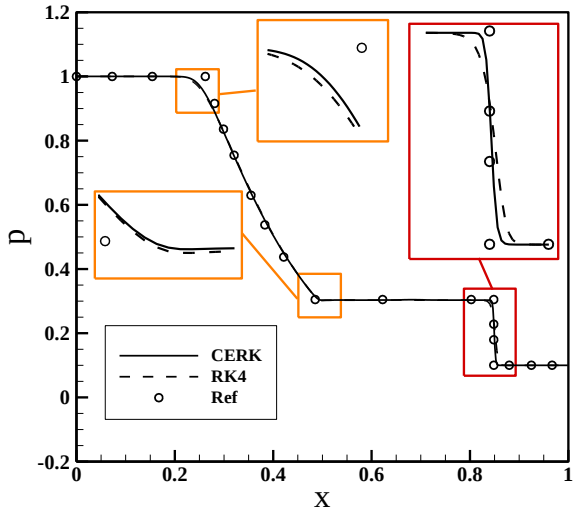

Fig. 4. Pressure variations in the Sod Riemann problem for first-order spatial discretization.

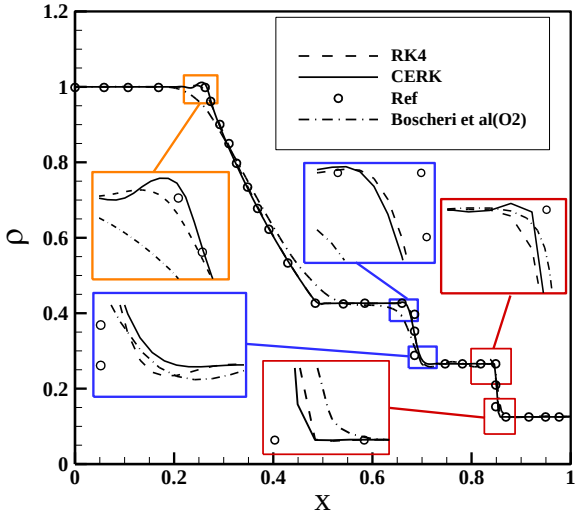

Fig. 5. density variations in the Sod Riemann problem for second-order spatial discretization.

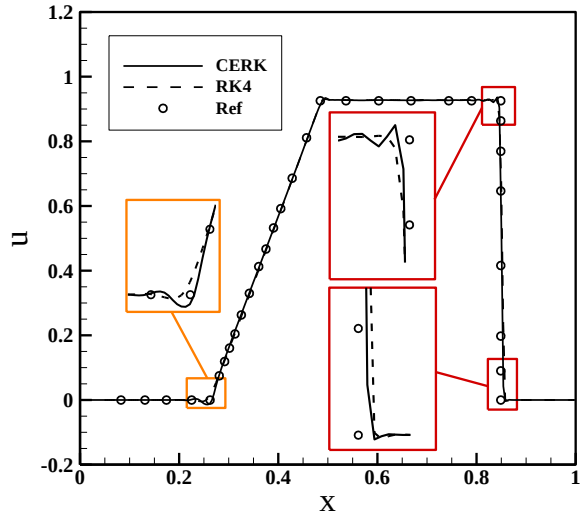

Fig. 6. velocity variations in the Sod Riemann problem for second-order spatial discretization.

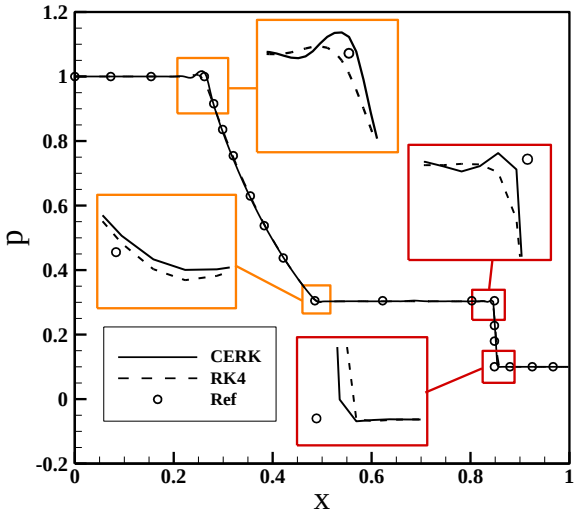

Fig. 7. pressure variations in the Sod Riemann problem for second-order spatial discretization.

To assess the implicit-explicit method's performance across various Mach numbers, our focus shifts to the acoustic wave problem, characterized by a low Mach number regime. Specifically, when $\varepsilon = 10^{-2}$ is employed in Fig. 1, the flow behavior becomes entirely incompressible. Fig. 8 through Fig. 12 present a comparison of pressure and momentum distribution results for the two temporal discretization methods in this problem. The presented figures illustrate outcomes from two scenarios of spatial discretization: first-order with 500 cells and second-order with 250 and 100 cells. These numerical results were validated and compared with the reference [38]. Notably,

density-based algorithms like the Roe method exhibit significant numerical dissipation errors at low Mach numbers due to dissipative terms (numerical dissipation Eq. (7)) leading to increased numerical diffusion and substantial computational errors [39]. However, in this context, the explicit-implicit method, with reduced numerical diffusion compared to the explicit fourth-order Runge-Kutta method, demonstrates enhanced accuracy. The explicit-implicit method ensures better alignment of the acoustic wave and contact interface propagation with the reference results. The pressure-velocity decoupling, stemming from the continuity equation, introduces stiffness in the equations. By employing implicit methods, the stability domain is extended, resulting in improved accuracy and reduced stiffness of the system of equations. With an increase in the spatial discretization order of the system of equations to second order, and consequently a reduction in numerical dissipation errors and dominance of dispersion errors, the implicit-explicit method is accompanied by wiggles in the vicinity of discontinuities. To address the issue of instability, there are two potential strategies to consider. The first approach involves reducing the time step, which effectively decreases the oscillations observed in the results, as demonstrated in Fig. 10. On the other hand, the second strategy involves reducing the grid density, leading to accurate solutions without oscillations, as illustrated in Fig. 11. Aligned with the Sod shock tube problem, the numerical outcomes derived from the investigation conducted by [16] for both first and second-order temporal and spatial discretization schemes, in the context of the low Mach number Riemann problem, are showcased in Fig. 8 and Fig. 12, respectively. These simulations entailed a computational grid comprising 500 elements, with results obtained utilizing the implicit-explicit method featuring a pressure-based formulation. The findings highlight that the approach employed in [23] for both first and second-order discretization gives rise to numerical dissipation and dispersion errors. Consequently, the accuracy and stability of the outcomes are compromised

compared to the results derived from the current study. Moreover, the presence of minor oscillations in the second-order spatial discretization of the present investigation, as depicted in F ig. 12, suggests the effective application of a suitable limiter in this research. Table 2 presents a comprehensive overview of the performance of two algorithms concerning their stability and CPU time. In this specific problem characterized by an extremely low Mach number and dominant system stiffness, the focus is on the performance of implicit-explicit methods, particularly in the incompressible regime. The stiffness of the equation system significantly impacts the maximum allowable time step of the fourth-order Runge-Kutta method in comparison to the semi-implicit approach. Conversely, the implicit-explicit method, even with first-order temporal discretization, offers advantages due to its semi-implicit formulation. As indicated in Eq. (3), the equivalent time step is smaller than the actual time step, resulting in reduced equation stiffness. This reduction permits the use of larger time steps within this method, leading to a significant decrease in CPU time consumption. Consequently, the time step increases by 66%, and CPU time decreases by 68% for first-order spatial discretization. For second-order spatial discretization, there is a noteworthy 72% reduction in computational cost.

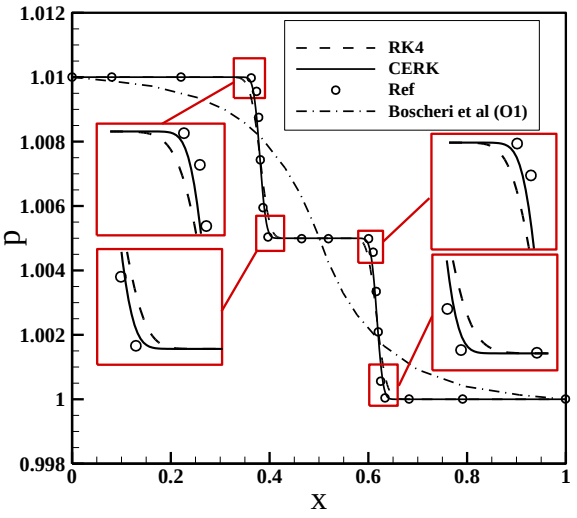

Fig. 8. pressure distribution in the low Mach Riemann problem for first-order spatial discretization.

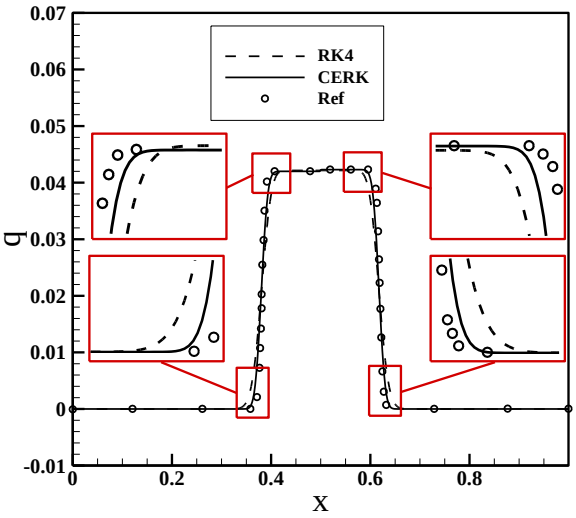

Fig. 9. momentum distribution in the low Mach Riemann problem for first-order spatial discretization.

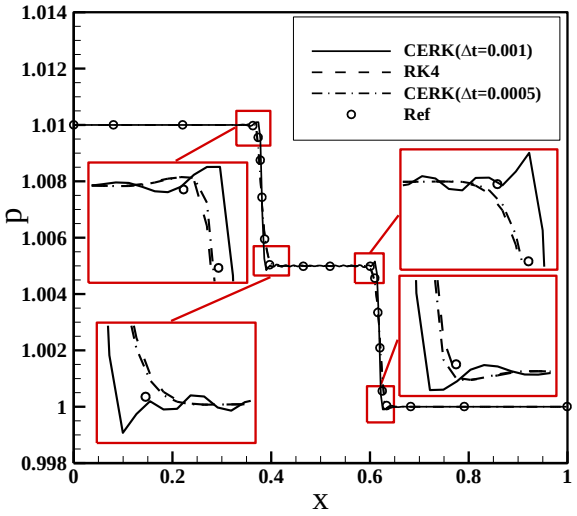

Fig. 10. pressure distribution in the low Mach Riemann problem for second-order spatial discretization.

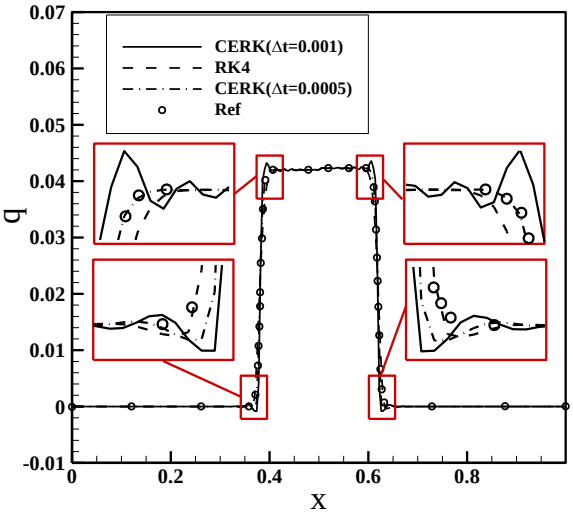

Fig. 11. momentum distribution in the low Mach Riemann problem for second-order spatial discretization.

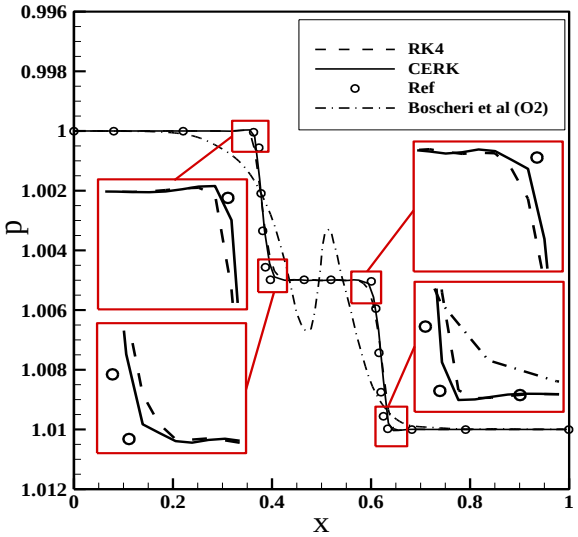

Fig. 12. momentum distribution in the low Mach Riemann problem for second-order spatial discretization with 100 cells.

4.2. Viscous 2D flow over circular cylinder

The steady viscous flow around a stationary cylinder serves as a recognized standard benchmark test case for evaluating and contrasting the accuracy and performance of employing an implicit-explicit numerical scheme against a fourth-order explicit Runge-Kutta method in simulating two-dimensional Navier-Stokes equations. Fig. 13 illustrates the schematic representation and

computational domain of a uniform flow encircling a cylinder with a diameter of one unit. For conducting this numerical simulation, an unstructured grid and domain with dimensions of 31.5 by 11.5 have been employed, comprising a total of 24,659 cells. Inoue and Hatakeyama [40] performed direct numerical simulations (DNS) to investigate the flow passing over a cylinder at Reynolds number 150 and Mach number 0.2. The outcomes of their simulation serve as a valuable resource for validation and comparative analysis within the scope of this present study. In this specific test case, the focus is on accurately capturing the wake regions. Therefore, only a spatial discretization method of second-order accuracy is considered. The cylinder wall is subjected to adiabatic and no-slip wall boundary conditions, while non-reflecting characteristic-based boundary conditions are applied at the far-field boundary. Fig. 14 displays the contour of instantaneous vorticity obtained from a numerical simulation using the fourth-order Runge- kutta and implicit-explicit method. It also illustrates the occurrence of vortex shedding in the wake zone of the cylinder. Accurate prediction of vortex shedding frequencies is of great importance in computational engineering analyses. Thus, the demonstrated precision of the recently developed method in forecasting these frequencies confirms its capacity to solve unsteady problems. In Fig. 15, a comparative analysis is conducted on the variations in the lift coefficient over time using different temporal schemes, along with the reference [40]. The results indicate a significant agreement between the numerical findings and the reference data. Additionally, in the analysis of vortex shedding, Table 1 presents the time-averaged mean values of the lift coefficient (C_{L0}) and drag coefficient (C_{D0}), as well as the amplitude of the lift coefficient (C_L) and the Strouhal number. These values are computed using the temporal discretization methods mentioned previously and are compared to the findings of Inoue and Hatakeyama [40]. The explicit-implicit method shows a maximum lift coefficient that closely approximated the reference values, as indicated by Fig. 15.

Table 1 provides a comparison of computational costs, including the maximum allowable time step and the corresponding physical time required to complete a unit of non-dimensional time. When comparing the fourth-order Runge-Kutta method to the explicit-implicit approach, the latter allows for a larger maximum time step (1.5 times larger); however, the explicit-implicit method significantly improves CPU time efficiency by reducing the required physical time by 38% to complete a unit of non-dimensional time.

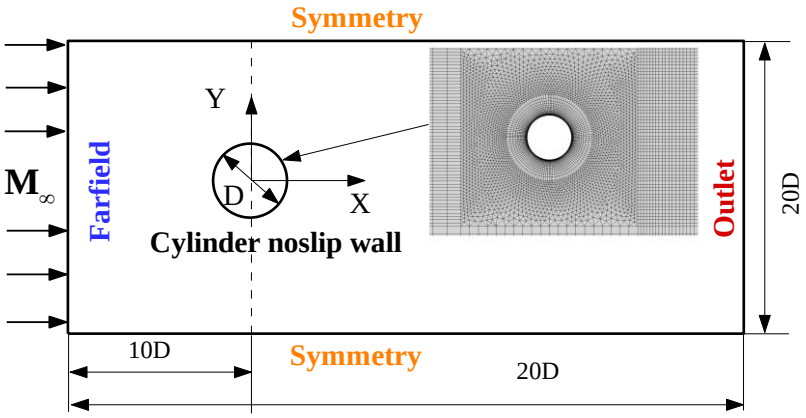

Fig. 13. A depiction of the flow around an immobile circular cylinder is displayed herein, characterized by a free-stream Reynolds number Re = 150 and a Mach number M = 0.2.

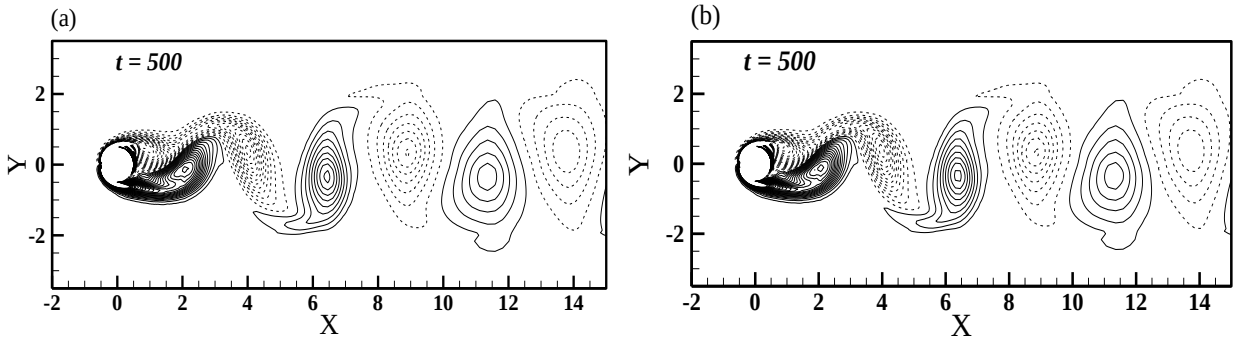

Fig. 14. Time development of a vorticity field. M = 0.2, Re = 150. The contour levels are from $\omega_{min} = -1$ to $\omega_{max} = 1$ with an increment of 0.04: ——, $\omega > 0$; – – –, $\omega < 0$. (a) CERK scheme, (b) RK4 scheme.

Table 1. comparison of aerodynamic coefficient and Strouhal number for differente temporal discretization.

Temporal discritization	C_{L0}	C_{D0}	C_L	St number
Inoue and Hatakeyama[40]	0	1.32	0.52	0.183
RK4	0	1.307	0.508	0.1814
CERK	0	1.3067	0.51	0.1814

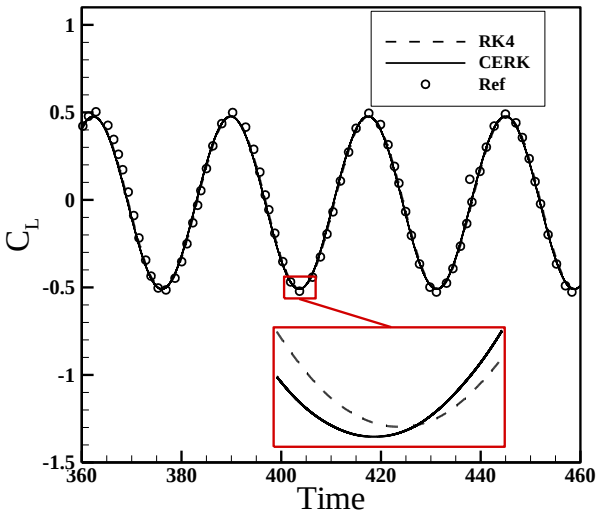

Fig. 15. Comparison of time-varying lift coefficient obtained from the proposed semi-implicit method with the .DNS results of Inoue and Hatakeyama [40] along with the results of Runge-Kutta scheme

Table 2. Comparing Computational Time and Maximum Allowable Time Step for Simulating Different Types of Problems

The Computational PC Information	Asus laptop with Core™ Intel® i7-4720HQ CPU @ 2.60 GHz & 8 GB RAM									
Test Case	SOD Riemann shock tube				Low Mach shock tube				flow over cylinder	
Scheme	CERK	RK4	CERK	RK4	CERK	RK4	CERK	RK4	CERK	RK4
Order in space	1	1	2	2	1	1	2	2	2	2
CPU time (s)	1	0.6	9	5	0.75	2.375	2.73	9.75	70	113
Maximum allowable time step	0.005	0.005	0.005	0.005	0.005	0.0003	0.001	0.001	0.0002	0.0003

5. Conclusion

This research presents the development of a novel first-order implicit-explicit time discretization method specifically designed for implementation with the upwind Roe density-based finite volume scheme on an unstructured grid. The primary objective of this advancement is to effectively address the computational stiffness associated with incompressible systems of equations. While the technique used is fundamentally implicit, it eliminates the need for calculating the inverse coefficient matrix or solving nonlinear equations; instead, the equations are resolved explicitly. The objective of this study was to evaluate the efficacy of the explicit-implicit

approach, commonly referred to as CERK. To achieve this, a series of benchmark problems were analyzed in one and two dimensions, with a specific focus on solving the Euler and Navier-Stokes equation systems in both compressible and incompressible regimes. These benchmark problems were compared to the fourth-order explicit Runge-Kutta technique to assess accuracy, stability, robustness, and computational cost. The one-dimensional Riemann Sod problem was utilized as a simulation benchmark for replicating the compressible flow regime. Conversely, the low Mach number Riemann problem was employed to simulate the incompressible flow regime and to investigate the effect of stiffness within the Euler equation system. Subsequently, the two-dimensional Navier-Stokes equations were employed to model the viscous flow around an incompressible cylinder. This was conducted while considering scenarios where the system's stiffness played a significant role in the governing equations. The subsequent analysis of the outcomes derived from these simulations has been systematically categorized as outlined below:

- In the context of the Riemann Sod problem, which falls under the category of high Mach number cases and features multiple numerical discontinuities, the implicit-explicit method demonstrated superior computational accuracy compared to the explicit Runge-Kutta method, particularly on coarse grids. This superiority can be attributed to the reduced numerical dissipation associated with the implicit-explicit method. However, when considering factors such as robustness and computational cost, the explicit Runge-Kutta method proved to be more advantageous

- In the case of the low Mach number Riemann problem, where factors such as an incompressible flow regime and the stiffness of the equation system are in focus, the efficacy of the Implicit-Explicit Runge-Kutta method has been observed with

considerable interest. Remarkably, enhancements are not confined to the precision of the method, but also extend to an extended stability domain. Moreover, the computational expense has significantly decreased, reaching up to 72%. These findings highlight the potential of the implicit-explicit method as a promising approach for efficiently and accurately simulating low Mach number problems

- By improving spatial accuracy, computational precision was enhanced for both temporal discretization methods. However, it was observed that the implicit-explicit method experienced numerical instabilities in regions with discontinuities, which resulted in a narrower stability domain for this numerical approach

- In the final examination, we focused on a pivotal test case that involves the simulation of the Navier-Stokes equations and the numerical solution for two-dimensional flow encircling a cylinder, with a Mach number of 0.2 and Reynolds number 150. Our inquiry extended beyond validation and involved a comprehensive comparison of numerical outcomes using the implicit-explicit method against the findings of other researchers. Significantly, this algorithm yielded a reduction of 38% in computational costs by effectively mitigating the equation system's stiffness.

References

[1] Alazard, T., Low Mach number limit of the full Navier-Stokes equations, Archive for rational mechanics and analysis, 180, 2006, 1-73.

[2] Colomés, O., Badia, S., Codina, R., and Principe, J., Assessment of variational multiscale models for the large eddy simulation of turbulent incompressible flows, Computer Methods in Applied Mechanics and Engineering, 285, 2015, 32-63.

[3] LeVeque, R.J., *Finite volume methods for hyperbolic problems*. Cambridge university press, 2002.

[4] Osher, S. and Solomon, F., Upwind difference schemes for hyperbolic systems of conservation laws, Mathematics of computation, 38, no. 158, 1982, 339-374.

[5] Dellacherie, S., Analysis of Godunov type schemes applied to the compressible Euler system at low Mach number, Journal of Computational Physics, 229, no. 4, 2010, 978-1016.

[6] Choi, D. and Merkle, C.L., Application of time-iterative schemes to incompressible flow, AIAA journal, 23, no. 10, 1985, 1518-1524.
[7] Djavareshkian, M.H., Moghadas Khorasani, M., and Mohammadi, A., Comparing the performance of preconditioning matrixes in wide range of internal and external flows, Fluid Mechanics & Aerodynamics Journal, 10, no. 2, 2022, 35-54.
[8] Li, X.-s. and Gu, C.-w., An all-speed Roe-type scheme and its asymptotic analysis of low Mach number behaviour, Journal of Computational Physics, 227, no. 10, 2008, 5144-5159.
[9] Li, X.-s. and Gu, C.-w., The momentum interpolation method based on the time-marching algorithm for all-speed flows, Journal of Computational Physics, 229, no. 20, 2010, 7806-7818.
[10] Liao, F. and Jin, Y., A preconditioned boundary-implicit subiterative DDADI method for the accuracy and efficiency enhancement in low-Mach number flows, Computers & Fluids,2023, 105950.
[11] Maia, A., Kapat, J., Tomita, J., Silva, J., Bringhenti, C., and Cavalca, D., Preconditioning methods for compressible flow CFD codes: Revisited, International Journal of Mechanical Sciences, 186, 2020, 105898.
[12] Darmofal, D. and Schmid, P., The importance of eigenvectors for local preconditioners of the Euler equations, Journal of Computational Physics, 127, no. 2, 1996, 346-362.
[13] Alkishriwi, N., Meinke, M., and Schröder, W., A large-eddy simulation method for low Mach number flows using preconditioning and multigrid, Computers & fluids, 35, no. 10, 2006, 1126-1136.
[14] Helenbrook, B.T. and Cowles, G.W., Preconditioning for dual-time-stepping simulations of the shallow water equations including Coriolis and bed friction effects, Journal of Computational Physics, 227, no. 9, 2008, 4425-4440.
[15] Myint-u, T., *Partial differential equations of mathematical physics*. CUP Archive, 1978.
[16] Ascher, U.M., Ruuth, S.J., and Wetton, B.T., Implicit-explicit methods for time-dependent partial differential equations, SIAM Journal on Numerical Analysis, 32, no. 3, 1995, 797-823.
[17] Ascher, U.M., Ruuth, S.J., and Spiteri, R.J., Implicit-explicit Runge-Kutta methods for time-dependent partial differential equations, Applied Numerical Mathematics, 25, no. 2-3, 1997, 151-167.
[18] Calvo, M., De Frutos, J., and Novo, J., Linearly implicit Runge–Kutta methods for advection–reaction–diffusion equations, Applied Numerical Mathematics, 37, no. 4, 2001, 535-549.
[19] Kupka, F., Happenhofer, N., Higueras, I., and Koch, O., Total-variation-diminishing implicit–explicit Runge–Kutta methods for the simulation of double-diffusive convection in astrophysics, Journal of Computational Physics, 231, no. 9, 2012, 3561-3586.
[20] Boscarino, S., Qiu, J., Russo, G., and Xiong, T., High order semi-implicit WENO schemes for all-Mach full Euler system of gas dynamics, SIAM Journal on Scientific Computing, 44, no. 2, 2022, B368-B394.
[21] Boscarino, S., Qiu, J.-M., Russo, G., and Xiong, T., A high order semi-implicit IMEX WENO scheme for the all-Mach isentropic Euler system, Journal of Computational Physics, 392, 2019, 594-618.
[22] Cordier, F., Degond, P., and Kumbaro, A., An asymptotic-preserving all-speed scheme for the Euler and Navier–Stokes equations, Journal of Computational Physics, 231, no. 17, 2012, 5685-5704.
[23] Boscheri, W., Dimarco, G., Loubère, R., Tavelli, M., and Vignal, M.-H., A second order all Mach number IMEX finite volume solver for the three dimensional Euler equations, Journal of Computational Physics, 415, 2020, 109486.
[24] Boscheri, W. and Pareschi, L., High order pressure-based semi-implicit IMEX schemes for the 3D Navier-Stokes equations at all Mach numbers, Journal of Computational Physics, 434, 2021, 110206.
[25] Boscheri, W. and Tavelli, M., High order semi-implicit schemes for viscous compressible flows in 3D, Applied Mathematics and Computation, 434, 2022, 127457.
[26] Boscheri, W., Dimarco, G., and Tavelli, M., An efficient second order all Mach finite volume solver for the compressible Navier–Stokes equations, Computer Methods in Applied Mechanics and Engineering, 374, 2021, 113602.
[27] Jiang, H. and Cheng, L., Flow separation around a square cylinder at low to moderate Reynolds numbers, Physics of Fluids, 32, no. 4, 2020
[28] Jiang, H. and Cheng, L., Hydrodynamic characteristics of flow past a square cylinder at moderate Reynolds numbers, Physics of Fluids, 30, no. 10, 2018
[29] Jiang, H. and Cheng, L., Transition to the secondary vortex street in the wake of a circular cylinder, Journal of Fluid Mechanics, 867, 2019, 691-722.
[30] Wang, J., Shan, X., and Liu, J., First instability of the flow past two tandem cylinders with different diameters, Physics of Fluids, 34, no. 7, 2022
[31] Yadav, V.S., Ganta, N., Mahato, B., Rajpoot, M.K., and Bhumkar, Y.G., New time-marching methods for compressible Navier-Stokes equations with applications to aeroacoustics problems, Applied Mathematics

and Computation, 419, 2022, 126863.
[32] Hoffmann, K.A. and Chiang, S.T., Computational fluid dynamics volume I, Engineering education system,2000
[33] Barth, T. and Jespersen, D., "The design and application of upwind schemes on unstructured meshes," in *27th Aerospace sciences meeting*, 1989, p. 366.
[34] Hairer, E., Wanner, G., and Solving, O., *II: Stiff and Differential-Algebraic Problems*. Berlin [etc.]: Springer, 1991.
[35] Spijker, M.N., Stiffness in numerical initial-value problems, Journal of Computational and Applied Mathematics, 72, no. 2, 1996, 393-406.
[36] Butcher, J.C., *Numerical methods for ordinary differential equations*. John Wiley & Sons, 2016.
[37] Jameson, A., Schmidt, W., and Turkel, E., "Numerical solution of the Euler equations by finite volume methods using Runge Kutta time stepping schemes," in *14th fluid and plasma dynamics conference*, 1981, p. 1259.
[38] Toro, E.F., *Riemann solvers and numerical methods for fluid dynamics: a practical introduction*. Springer Science & Business Media, 2013.
[39] Guillard, H. and Viozat, C., On the behaviour of upwind schemes in the low Mach number limit, Computers & fluids, 28, no. 1, 1999, 63-86.
[40] Inoue, O. and Hatakeyama, N., Sound generation by a two-dimensional circular cylinder in a uniform flow, Journal of Fluid Mechanics, 471, 2002, 285-314.